Volume 6
Number 21
7 November 2025
Pages 7621–8194

Materials Advances

rsc.li/materials-advances

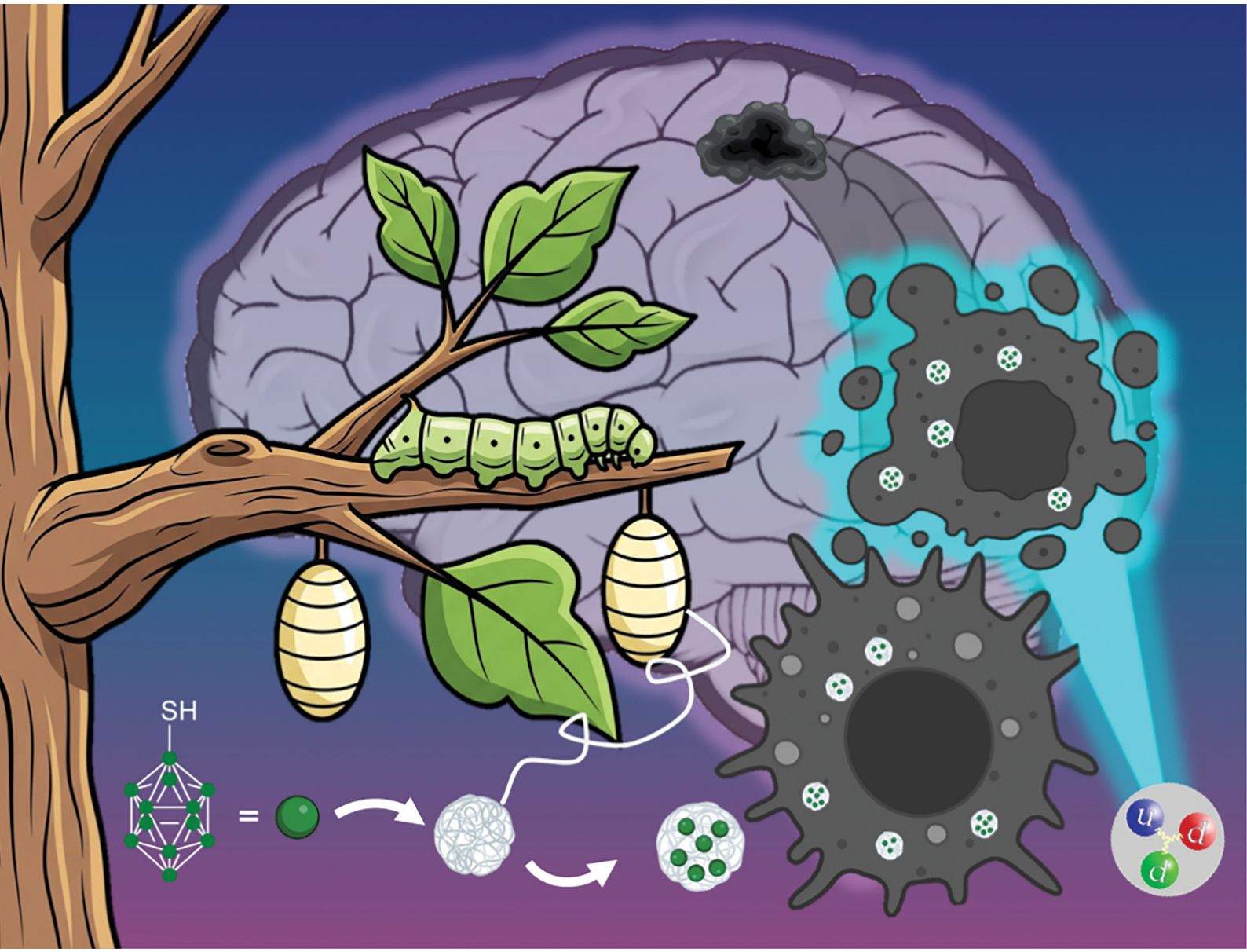

ISSN 2633-5409

ROYAL SOCIETY OF CHEMISTRY

PAPER
Ivana Miletto, Daniela Imperio *et al.*
In vitro delivery of borocaptate ions to U87 glioma cells *via* silk fibroin nanoparticles for boron neutron capture therapy

Materials Advances

ROYAL SOCIETY OF CHEMISTRY

PAPER

View Article Online
View Journal | View Issue

Cite this: *Mater. Adv.*, 2025, 6, 7791

In vitro delivery of borocaptate ions to U87 glioma cells *via* silk fibroin nanoparticles for boron neutron capture therapy

Elia Bari, †[a] Ian Postuma,†[b] Ivana Miletto, *[a] Daniela Imperio, *[c] Silva Bortolussi, [db] Laura Cansolino, [eb] Cinzia Ferrari, [eb] Yuan-Hao Liu, [fgh] Yuan Zhenwei, [i] Maria Luisa Torre [a] and Luigi Panza [a]

Received 7th April 2025,
Accepted 15th August 2025

DOI: 10.1039/d5ma00336a

rsc.li/materials-advances

Boron neutron capture therapy (BNCT) is an oncological treatment based on the neutron capture reaction on ^{10}B. The only two compounds approved for phase I/II clinical trials are sodium borocaptate (BSH) and 4-boronophenylalanine (BPA). While BPA has been widely exploited in clinical trials, the use of BSH is limited due to its insufficient uptake by tumor cells. Herein, we report a novel formulation based on silk fibroin nanoparticles (SFNs), capable of loading a large amount of borocaptate ions. The nanoparticles have been characterized and tested on U87 glioma cells, and boron uptake was measured using neutron autoradiography, which involved irradiating the samples in a thermal neutron field. Measurements demonstrated the crucial role of the nanocarrier in enhancing boron internalization. Notably, SFNs-BSH achieved 29.5 ppm total boron uptake in U87 cells – comparable to clinical BPA – at 4× lower dose.

1. Introduction

Boron neutron capture therapy (BNCT) is a promising binary radiotherapeutic approach to cancer treatment. It involves administering two agents simultaneously: a boron-containing compound and a high-flux beam of low-energy neutrons. The combination of these two components produces a highly cytotoxic effect on boron-containing cells. The mechanism occurs when a ^{10}B nucleus captures a neutron, triggering a nuclear capture reaction that generates an alpha particle and a lithium-ion; these are low-range, high-linear energy transfer particles that release their energy within the cells, effectively destroying them. For optimal therapeutic results, irradiation should be performed when the boron concentration within the tumor tissue is as high as possible, with 20 ppm of boron considered the minimum therapeutic concentration to achieve a therapeutic dose, given the neutron beam currently available for therapy. Additionally, a sufficient boron concentration ratio between the tumor and healthy tissues is necessary to minimize damage to neighboring cells.[1]

A primary challenge in BNCT development has been the availability of neutron sources that can generate a high neutron flux with proper characteristics: an epithermal spectrum peaked between 1 and 10 keV and with minimal spectral components at lower and higher energies. Until about ten years ago, only research nuclear reactors could meet these requirements; however, the recent availability of accelerators delivering high proton currents coupled with beryllium or lithium targets, which generate a neutron beam, has caused a paradigm shift in BNCT. A significant milestone came in 2020 with the installation of Japan's first accelerator-based neutron source at Southern Tohoku General Hospital in Koriyama (Fukushima Prefecture). This facility became the first to treat patients using such technology, and as a result, BNCT is now offered as a National Health System therapy in Japan.[2] Since then, additional companies have entered the field, supplying accelerators for BNCT, while public research institutions have driven the development of new machines in multiple countries.[3]

The advent of these new accelerators has sparked research into developing new boron carriers, a field that is still in its

[a] *Department of Pharmaceutical Sciences, University of Eastern Piedmont, Largo Guido Donegani, 2, 28100, Novara, Italy. E-mail: ivana.miletto@uniupo.it*
[b] *National Institute of Nuclear Physics (INFN), Unit of Pavia, via A. Bassi 6, 27100, Pavia, Italy*
[c] *Department for Sustainable Development and Ecological Transition, University of Eastern Piedmont, Piazza Sant'Eusebio 5, 13100, Vercelli, Italy. E-mail: daniela.imperio@uniupo.it*
[d] *Department of Physics, University of Pavia, via A. Bassi 6, 27100, Pavia, Italy*
[e] *Department of Clinical Surgical Sciences, Integrated Unit of Experimental Surgery, Advanced Microsurgery and Regenerative Medicine, University of Pavia, via Ferrata 9, 27100, Pavia, Italy*
[f] *Neuboron Therapy System Ltd, Xiamen, 361028, China*
[g] *Nanjing University of Aeronautics and Astronautics, Nanjing, 210016, China*
[h] *Neuboron Medtech Ltd., Nanjing, 211112, China*
[i] *Department of Biomedical Engineering, School of Engineering China Pharmaceutical University 639, Longmian Road, Jiangning District Nanjing, 210009, China*
† E. B. and I. P. contributed equally to the manuscript.

infancy despite long and extensive efforts. Indeed, to date, only three boron-containing molecules have been approved in clinical trials, but only one has entered the market for treatment,[4] although it is far from ideal.[5] In particular, the only two compounds approved for phase I/II clinical trials are BSH and BPA. Borofalan (^{10}B), a novel formulation of BPA, has been recently approved in Japan, where BNCT is now included for coverage by the national health insurance system for unresectable locally advanced or locally recurrent head and neck cancer. New boron agents should have optimal tumor selectivity, prolonged retention within tumor tissues, stability in the bloodstream, ensuring they remain effective until they reach the target cells, and reduced clearance by the liver and kidneys to reduce potential toxicity.[6] Consequently, researchers have developed a range of boron-containing agents for BNCT,[7] exploiting different classes of compounds as targeting moieties for selective tumor accumulation. These include carbohydrates,[8–12] amino acids and small peptides,[13] nucleobases[14] porphyrins,[15] 2-nitroimidazole derivatives,[16–18] and DNA intercalators.[19]

With improved delivery mechanisms, nanomedicine also holds promise for targeted BNCT treatment. Nanoparticles, due to their small size, can easily cross cell membranes, facilitating intracellular drug delivery even for molecules poorly absorbed by tumor cells.[20,21] They enhance drug protection, reduce clearance for easily degradable drugs, and enable controlled drug release at specific sites, improving treatment efficacy and reducing side effects.[22] This targeted approach can be achieved through passive targeting, relying on the enhanced permeability and retention effect, allowing nanoparticles to accumulate in areas with altered vascularization,[23] or active targeting by functionalizing them with ligands that interact with receptors on the target tumor cells.[24] As such, recently, various nanoparticles have been explored as boron delivery agents, including boron metal cores, and boron carbides, mesoporous silica nanoparticles,[25] polymeric nanoparticles,[26] and vesicles,[27] with a focus on liposomes.[28] Glioblastoma (GBM) typically recurs at the site of origin, highlighting the need for more intensive and tumor-selective therapeutic strategies.[29] In the past, numerous liposomal formulations have been developed to improve the delivery of the already-mentioned BSH, for example, epidermal growth factor receptor (EGFR), a transmembrane tyrosine kinase overexpressed in human glioblastoma, has been exploited as a promising target for BSH selective delivery.[30] However, finding the right lipid composition is sometimes trivial and expensive. Biodegradable Periodic Mesoporous Organosilicas (BMPO) containing BSH have been developed; nevertheless, BSH-BPMO nanoparticles production required several synthetic steps and the surface of these particles has to be modified to introduce reactive moieties for the BSH grafting.[31]

To date, few studies have used nanoparticles generated solely from natural biocompatible polymers,[32] and none have utilized silk fibroin (SF), a protein extracted from silkworm silk.

SF is a highly versatile candidate for the preparation of nanoparticles, not requiring the use of toxic and expensive cross-linking agents,[33] being compatible with standard sterilization methods,[34] exhibiting biodegradability, biocompatibility, and low immunogenicity,[35] and inducing a lower inflammatory response compared to widely used synthetic polymers, such as polylactic acid.[36] Silk fibroin nanoparticles (SFNs) encapsulate a wide variety of hydrophilic and lipophilic compounds, and their surface functional groups allow easy functionalization to provide active targeting.[37–42] For example, SFNs derivatized with RGD-based cyclic pentapeptides have shown selective binding to $\alpha\beta\nu3$ and $\alpha\beta\nu5$ integrin subtypes, which are overexpressed in malignant cells.[43,44] Ultimately, the potential for translating SFNs from laboratory research to clinical applications shows promise due to the possibility of producing them with good manufacturing practices (GMP) and large-scale manufacturing processes.[45]

In this work, SFNs encapsulating sodium mercaptoundecahydro-*closo*-dodecaborate (or borocaptate, BSH) or tetramethylammonium BSH (hereafter N-BSH) were prepared, characterized, and tested (Scheme S1). BSH and N-BSH differ in their counterion (Fig. 1) and, therefore, in their solubility properties. Cellular uptake tests were performed on human GBM cell cultures (U87), and the concentration of internalized boron was measured by neutron autoradiography, a technique that allows for high-resolution quantification of boron at a relatively low cost. Neutron autoradiography is valuable in BNCT because it provides comprehensive information on boron uptake in biological samples. This technique enables the quantification and imaging of boron distribution in cell pellets, isolated cells, and tissue sections by detecting neutron capture products without destroying the samples. Understanding the uniformity of boron distribution is essential, as it indicates the effectiveness of the carrier in targeting all cells within a population, which anticipates the possibility of destroying all cancer cells within a tumor. Additionally, analyzing the lack of uniformity in boron distribution can inform improvements in the solubility and biocompatibility of new formulations. The quantification method based on grayscale mapping, which has already been assessed for molecules, was extended to the present formulations, highlighting the versatility and potential of this technique. Quantification can reach as low as 1 $\mu g\ g^{-1}$ (1 ppm) of ^{10}B and can be further explored at the subcellular level.[46]

2. Results and discussion

Boron neutron capture therapy relies on the capture of neutrons by boron to induce the death of tumor cells. As such, effective delivery of adequate boron quantities into the tumor

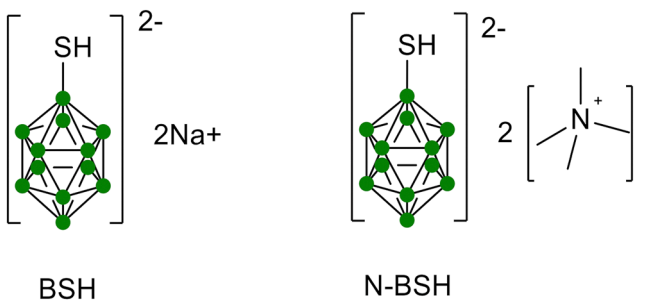

Fig. 1 Structures of sodium BSH (sodium mercaptoundecahydro-*closo*-dodecaborate, BSH) and tetramethylammonium BSH (tetramethylammonium mercaptoundecahydro-*closo*-dodecaborate, N-BSH) (green dots represent B atoms).

cells is crucial for maximizing therapeutic outcomes. Nowadays, BSH (Fig. 1) represents one of the compounds currently available clinically.[47] This boron carrier penetrates tumor tissue, but it accumulates insufficiently in the cancer cells.[47] On the other hand, compared to the drug used in clinics (boronophenylalanine, BPA), BSH offers the advantage of providing twelve boron atoms per molecule instead of one. Therefore, delivering a higher concentration of BSH to the tumor by exploiting innovative approaches is potentially very appealing. The BSH can be commercially obtained with some counterions; in particular, this study employs sodium-BSH (Fig. 1, BSH), which is water-soluble, and tetramethylammonium-BSH (Fig. 1, N-BSH), soluble in organic solvents such as acetone.

2.1. Preparation and characterization of SFNs-BSH and SFNs-N-BSH

The aforementioned boron carrier salts were encapsulated within SFNs to enhance their uptake by tumor cells. In recent years, SFNs emerged as a valid drug delivery system, being low-cost, biocompatible, and easily internalized by cells. The SFN preparation method involves the coacervation of an SF aqueous solution using an organic solvent, such as acetone. This process reduces the hydration of SF chains, causing SF protein to precipitate in the form of nanoparticles, while simultaneously forming β-sheet structures that trap the drug within the protein matrix.

The process yield % was 69.1% for SFNs-BSH and 70.5% for SFNs-N-BSH; these results align with our previous work[33,43,44,48] and are acceptable for laboratory-scale batch preparation. The residual humidity of freeze-dried SFNs never exceeded 3%, indicating a successful lyophilization process.

Semi-quantitative elemental composition was investigated by EDX (Energy Dispersive X-ray spectroscopy) analysis (Table 1 and Fig. S1 in SI). In both samples, boron is detected, confirming the successful loading of the BSH derivatives. The presence of carbon (C), nitrogen (N), oxygen (O), and sulfur (S), related to the protein composition, displayed an increased relative amount of S, due to the loading of BSH derivatives. In the case of SFNs-N-BSH, the relative amount of N and C is perturbed as well, due to the tetramethylammonium ions present in the N-BSH. When BSH is used, Na is found in the elemental composition of the loaded SFNs, as expected. The loading value of boron (B) is significantly higher in SFNs-BSH with respect to SFNs-N-BSH, indicating that loading BSH from the aqueous phase leads to a higher encapsulation efficiency.

Table 1 Elemental composition by EDX analysis

	Element	Wt%	Atomic%
SFNs-BSH	B	17.0	20.77
	C	45.9	50.32
	N	11.4	10.71
	O	16.9	13.91
	Na	4.0	2.30
	S	4.8	1.99
	Total	100.00	100.00
SFNs-N-BSH	B	6.31	7.56
	C	59.82	64.52
	N	11.53	10.66
	O	20.31	16.45
	S	2.03	0.82
	Total	100.00	100.00

The actual amount of encapsulated boron was quantified by ICP-OES (Inductively Coupled Plasma – Optical Emission Spectroscopy) analysis. As expected, the water-soluble derivative (BSH) was encapsulated with higher efficiency compared to the N-BSH, as it is non-soluble in acetone and is therefore better retained within the SF alongside the matrix during the desolvation process. The boron content of nanoparticles was calculated using ICP-OES, yielding values of 0.37 mgB mg^{-1} SFN-BSH for SFNs-BSH and 0.12 mgB mg^{-1} SFN-N-BSH for SFNs-N-BSH.

Field emission scanning electron microscopy (FE-SEM) morphological investigation of SFNs-BSH and SFNs-N-BSH showed that both samples have a round-shape morphology (Fig. 2A–D) and exhibit a good size homogeneity, which was further confirmed by nanoparticle tracking analysis (NTA) (Fig. 2E and F). No significant differences between loaded SFNs and bare SFNs were found (Fig. S2 in the SI), confirming that the SFNs formation by the desolvation method is not affected by the presence of the BSH/N-BSH, neither in the water nor in the acetone phase.

ζ-potential of SFNs-BSH and SFNs-N-BSH was measured in PBS buffer (0.01 M, pH 7.4), obtaining respectively of −6.29 mV ± 0.87 mV and −0.556 mV ± 0.079 mV, showing an influence of the entrapped BSH molecules and their positive counterions, as expected.[43]

ATR-IR (Attenuated Total Reflection Infrared) spectra of SFNs-BSH and SFNs-N-BSH were acquired and compared to the spectra of unloaded SFNs and the free compounds, and are reported in Fig. 3. All the SFNs showed the characteristic signals of amide A (3280 cm^{-1}, νN–H), amide I (at about 1616 cm^{-1}, δC═O), amide II (at about 1509 cm^{-1}, δN–H + νC–N), and amide III (at about 1230 cm^{-1}, νC–N + δN–H), as a further indication that the loading of mercaptododecaborate derivatives does not affect the formation of SFNs. FTIR spectra of mercaptododecaborate derivatives (Fig. 3, curves d and e) are dominated by the characteristic intense signal at 2479 cm^{-1}, ascribed to the stretching mode of the B–H bond. At lower frequencies, below 1200 cm^{-1}, a set of signals associated with vibrational modes of the icosahedral cage are present, which are typical of mercaptododecaborate derivatives (*e.g.*, d B–B–H *ca.* 1066 cm^{-1} in BSH and 1042 cm^{-1} in N-BSH; B–B cage vibration and breathing modes at 1005, 860, and 737 cm^{-1}).[49,50] Because of its high intensity and location in a spectral region (2600–2100 cm^{-1}) where SF shows no absorption, the stretching mode of the B–H bond at 2479 cm^{-1} is often utilized to confirm the presence of mercaptoborate derivatives and, more importantly, to conduct semi-quantitative evaluations.[51] Normalizing the SFNs spectra based on the amount of protein (using the amide I peak as a reference) enables the comparison of SFNs-BSH and SFNs-N-BSH samples regarding their mercaptododecaborate content. The integrated area of the 2479 cm^{-1} peak of the

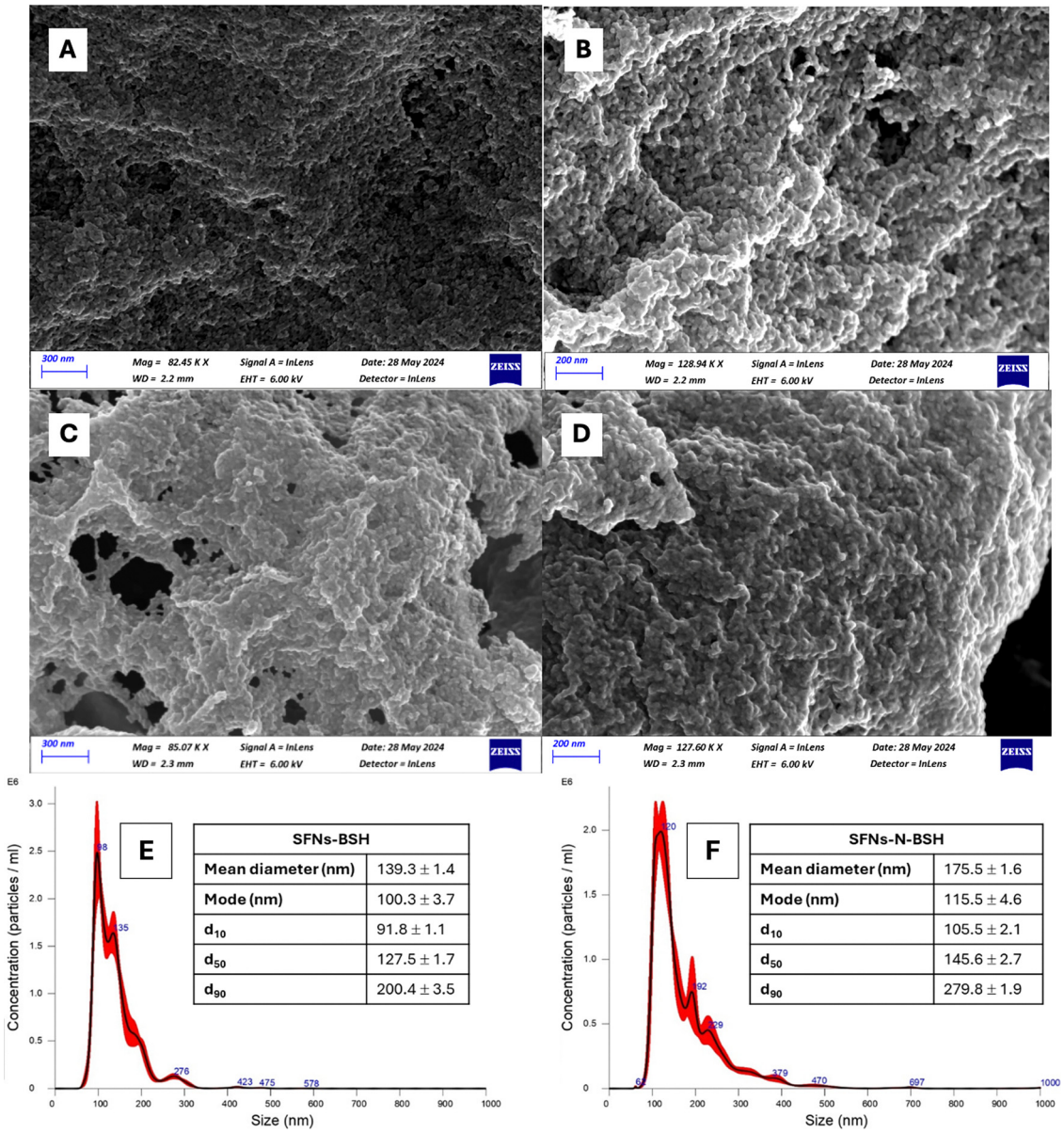

Fig. 2 Representative FE-SEM images of SFNs-BSH (A) and (B) and SFNs-N-BSH (C) and (D). Scale bars are of 300 nm (A) and (C) and 200 nm (B) and (D). Concentration plots from NTA for SFNs-BSH (E) and SFNs-N-BSH (F).

SFNs-BSH sample is *ca.* four times higher than that of SFNs-N-BSH spectrum, evidencing a significantly higher amount of the active in SFNs-BSH, in good agreement with the quantification made by EDX and ICP-OES analyses.

As previously mentioned, during the desolvation process, the drug becomes entrapped within the protein matrix that forms as SF precipitates into nanoparticles. Previous findings indicate that due to the compact nature of β-sheets, the diffusion of the entrapped drug through the protein matrix is significantly slower than cellular internalization,[44] especially if the molecular weight is high (219.87 g mol^{-1} and 322.18 g mol^{-1} for BSH and N-BSH, respectively). This assumption was confirmed through release studies (Fig. 4). Both formulations exhibited a gradual release of the active compound, reaching a plateau after 8 hours. The total amount of drug released was approximately 11.5% and 17.2% for SFNs-BSH and SFNs-N-BSH, respectively. This limited release is likely due to the burst release of the drug adsorbed on the nanoparticle surface. Consequently, given the low percentage of drug released over 24 hours, the encapsulated compound is expected to remain within the nanoparticles during circulation and cellular uptake, thereby promoting the effective accumulation of boron in tumor cells.

Finally, the suitability of SFNs for parenteral use, following their reconstitution in physiologic solution, was demonstrated by measuring the osmolarity value (comprised between 325 and 360 mOsm kg^{-1}) and the pH values (in the range of 7.2–7.6).

2.2. *In vitro* cytocompatibility and evaluation of boron uptake

Both formulations were tested for cytocompatibility on tumor (U87 glioma cells) and healthy (human dermal fibroblasts) cells in the range 200–800 μg mL^{-1}. SFN-BSH and SFN-N-BSH proved

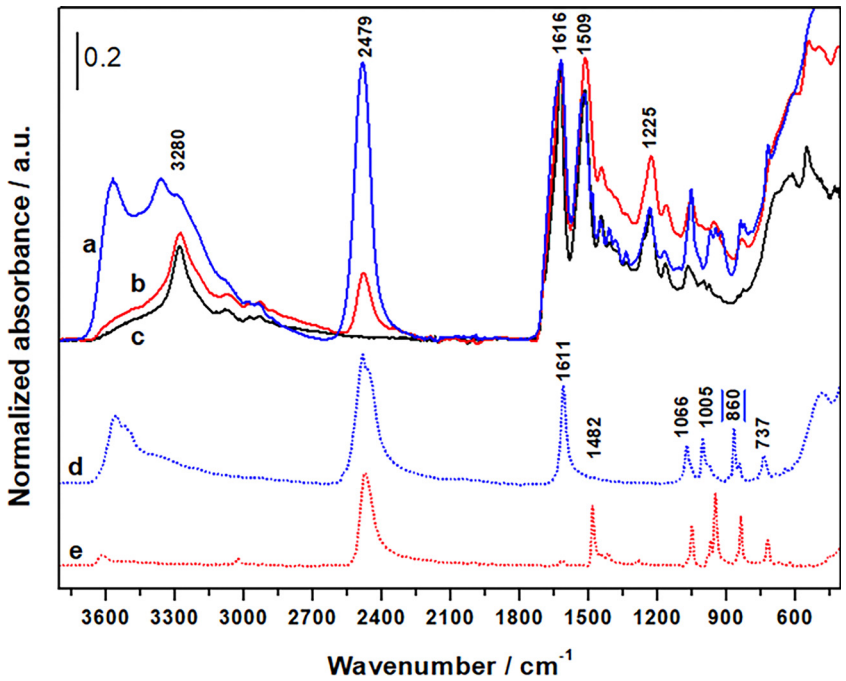

Fig. 3 ATR-FTIR spectra of SFN-BSH (solid blue, curve a), SFN-N-BSH (solid red, curve b), unloaded SFNs (solid black, curve c), reference compound BSH (dotted blue, curve d), and N-BSH (dotted red, curve e).

to be cytocompatible, as the cell viability was higher than 80% for all the concentrations tested (Fig. 5). The concentration of 400 μg mL^{-1} was selected for the subsequent uptake experiments on U87 glioma cells.

The neutron autoradiography technique was used to generate boron distribution maps in U87 human glioblastoma cell pellets and to measure boron concentration in samples following internalization of SFNs-BSH and SFNs-N-BSH. Fig. 6 shows the boron concentration in the cell pellets transformed into a color scale and reports the quantification by grayscale density measurements. Quantification was obtained by mapping the grayscale density of tracks and converting it into boron concentration based on calibration with standard samples, as reported in the Materials and methods section; the data are presented in Table 2.

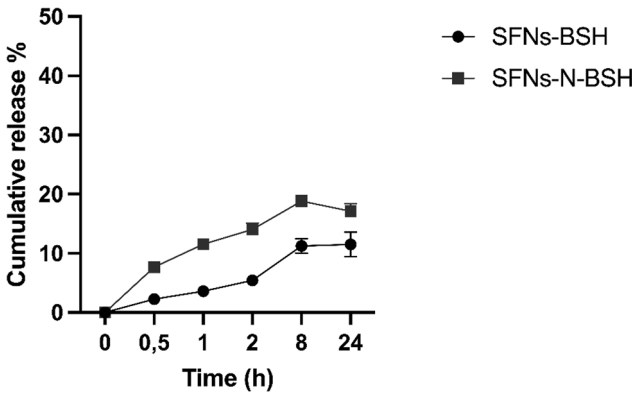

Fig. 4 Cumulative release % of BSH and N-BSH from nanoparticles immersed in pH 7.2 phosphate-buffered saline (PBS) at room temperature. Data are reported as mean values ± standard deviation, n = 3.

The measurements performed on control samples resulted in values below the detection limits, indicating a correct procedure in sample preparation. Cells exposed to SFNs-BSH exhibit a higher boron uptake than those exposed to SFNs-N-BSH. However, these results must be interpreted in relation to the boron concentration available in the culture medium. In both cases, cells were exposed to a solution containing 400 μg mL^{-1} of the formulation, resulting in boron concentrations of 150 ppm for SFNs-BSH and 50 ppm for SFNs-N-BSH. This corresponds to a concentration factor (boron taken up/boron provided up) of approximately 20% for SFNs-BSH and 17% for SFNs-N-BSH, indicating that SFNs-BSH performs more efficiently, the difference being relatively small. These data can be compared to boron uptake in the same cell line when treated with BPA, the boron formulation used in clinical BNCT. Under typical conditions, cells are exposed to a BPA-enriched medium containing 80 ppm of boron, resulting in a boron concentration of approximately 20 ppm (a concentration factor of about 25%). The tested nanoparticles demonstrated comparable efficiency to established molecules. However, achieving 80 ppm of boron in a culture medium requires 1.67 mg mL^{-1} of BPA (see Fig. S3 in SI), whereas only 400 μg mL^{-1} of SFNs-BSH – corresponding to 226 μg of loaded BSH – is needed to reach 150 ppm. This is a promising preliminary result, as one of the key limitations of clinical BNCT is the lengthy infusion process required for BPA administration, necessitating a dose of at least 350 mg kg^{-1} body weight for effective therapy.

3. Conclusion

In this work, the use of SFNs for BSH delivery is described. SFNs were shown to be efficient in loading borocaptate ions; in

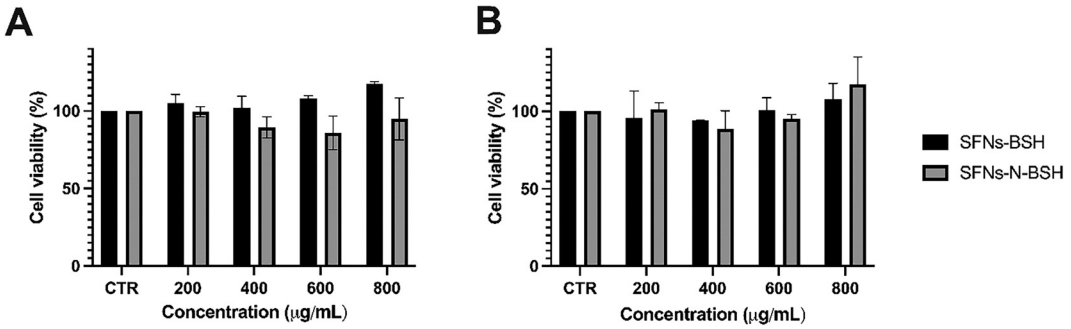

Fig. 5 Cell viability of U87 glioma cells (A) and human dermal fibroblasts (B) treated with SFN-BSH and SFN-N-BSH for 24 hours. CTR were cells not treated (100% viability).

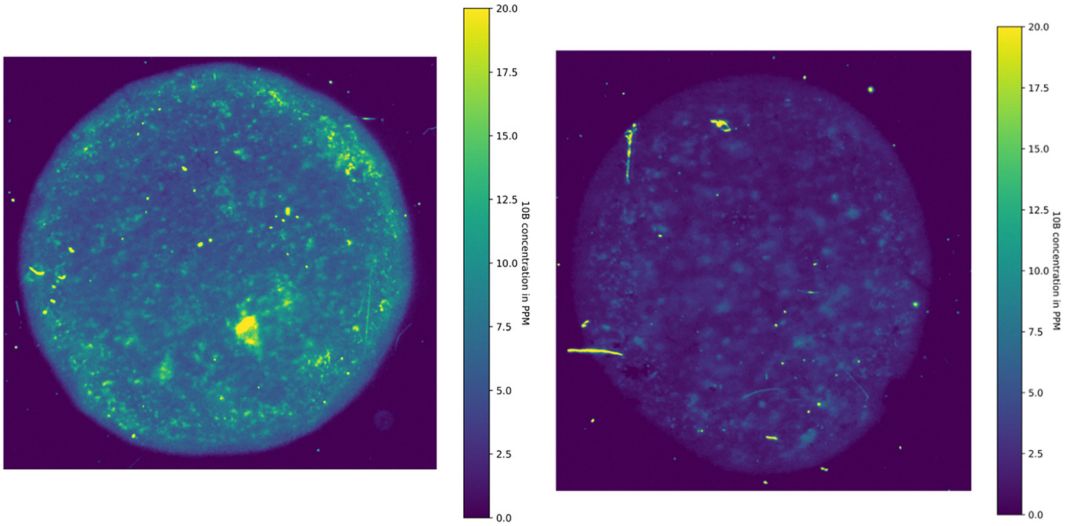

Fig. 6 Representative examples of the boron concentration in the cell pellets transformed into a color scale. Left: Example of uptake measurement and imaging for SFNs-BSH average ^{10}B concentration equal to 6.2 ± 0.9 ppm (instrumental uncertainty). Right: Example of uptake measurement and imaging for SFNs-N-BSH– average ^{10}B concentration equal to 1.6 ± 0.4 ppm (instrumental uncertainty). The small bright spots (background noise) were removed before further analysis.

particular, the loading of BSH in SFNs is much more efficient than that of N-BSH. Uptake experiments demonstrated that SFNs can transport the boron compound in U87 tumor cells more efficiently than BSH alone. Moreover, the amount of boron measured through the autoradiography technique reported promising results, registering a boron content comparable with that obtained by administering a four times higher dose of BPA to cell cultures. These results pave the way for the *in vivo* study of these novel formulations.

Table 2 ^{10}B concentration obtained by neutron autoradiography of cell pellets deposited on CR-39 detectors

Sample	^{10}B concentration [ppm]	Uncertainty [ppm]	Total boron concentration [ppm]
Ctr	<0.5	0.5	—q
SFNs-BSH	5.9	0.8	29.5
Ctr	<0.5	0.5	—
SFNs-N-BSH	1.7	0.5	8.5
BPA[a]	14.0	2.0	14.0

The results are the average of ^{10}B concentration in μg g^{-1} [ppm] in cell cultures treated with SFNs-BSH and SFNs-N-BSH, respectively (n = 3). The total boron concentration was calculated considering that 10B accounts for 20% of the total boron and that neutron autoradiography only detects ^{10}B. [a] Example of a previous experiment with BPA, 99.9% isotopic enrichment, at ^{10}B concentration of 80 ppm for 4 hours contact time, see SI for more information.

4. Materials and methods

4.1. Materials

Sodium mercaptododecaborate (BSH, 219.87 g mol^{-1}) and tetramethylammonium mercaptododecaborate (N-BSH, 322.18 g mol^{-1}) were purchased from Katchem spol. Sr.o. (Prague, Czech Republic). Lithium bromide (LiBr), sodium carbonate (Na_2CO_3), and sodium chloride (NaCl) were purchased from Merck (Milan, Italy). Acetone, hydrogen peroxide, nitric acid, perchloric acid, and 70 μm nylon meshes were purchased from VWR International (Milan, Italy). The dialysis cellulose tubes (molecular weight cutoff of 3.5 kDa) were

bought from Spectrum Laboratories (Milan, Italy). *Bombyx mori* cocoons were kindly donated by Nembri Industrie Tessili (Capriolo, Italy). Dulbecco's modified Eagle Medium (DMEM) was purchased from Lonza (Milan, Italy), while fetal bovine serum (FBS), gentamicin, and phosphate-buffered saline (PBS) were from Euroclone (Milan, Italy). Unless otherwise specified, all reagents were of analytical grade and used as such without dilution.

4.2. Preparation and characterization of SFNs

4.2.1. SF extraction. SF was separated from sericin through a degumming procedure. Briefly, *Bombyx mori* cocoons were cut into 1 × 1 × 1 cm pieces and boiled in water with Na_2CO_3 0.02 M for 30 minutes. Then, the SF fibers were repeatedly washed with warm deionized water, allowed to dry at room temperature, and then solubilized in 9.3 M LiBr at 65 °C for 4 hours (25% w/v concentration). The obtained SF solution was filtered through a 70 μm nylon mesh and then dialyzed against distilled water at room temperature for 72 hours. The final concentration of the SF solution was determined gravimetrically by freeze-drying known volumes and was 7.86% w/v.

4.2.2. SFNs preparation. SFNs were prepared by exploiting SF desolvation in acetone, according to procedures previously published.[33,43,44,48] The SF solution was diluted with deionized water to reach the concentration of 1.5% w/v and then added dropwise to acetone; the fibroin/acetone volume ratio was 1 : 5. To prepare SFNs-BSH, BSH was solubilized in the fibroin solution at 4.5 mg mL^{-1}, while for SFNs-N-BSH, the borocaptate was solubilized in acetone at 0.8 mg mL^{-1}. Unloaded SFNs were prepared as a reference for the chemical-physical characterization (see Section 4.2.3). The obtained nanoparticle suspension was dialyzed against distilled water at room temperature for 72 hours, collected, and then freeze-dried at a pressure of 8 × 10^{-1} mbar and a temperature of −50 °C for 72 hours (Modulyo® Edwards Freeze dryer, Kingston, NY, 27 USA).

4.2.3. SFNs characterization. The freeze-dried SFNs were characterized as reported below. Unless otherwise specified, each measurement was carried out in triplicate.

The yield % was calculated according to the equation:

$$\text{Yield\%} = \frac{\text{weight of nanoparticles}}{\text{weight of fibroin} + \text{weight of drug}} \times 100 \qquad (1)$$

The drug loading was verified by ICP-OES (Spectro Genesis ICP-OES simultaneous spectrometer by SPECTRO Analytical Instruments GmbH, Kleve, Germany). SFNs-BSH and SFNs-N-BSH (8 mg each) were digested in 0.3 mL of 70% perchloric acid and 0.6 mL of 30% hydrogen peroxide at 100 °C for 1 hour. The mixtures were then diluted to 10 mL in 1% v/v nitric acid.

SFNs' micro-analytical composition was also assessed by EDX analysis, carried out on a FEG-SEM TESCAN S9000 G (Brno – Kohoutovice, Czech Republic) instrument equipped with Ultim Max microanalysis detector and AZTEC Software (Oxford Instruments, High Wycombe, UK). Before the analysis, the samples were Cr-sputter-coated under argon.

The dimensional distribution of SFNs was analyzed using NanoSight NS300 equipment (Malvern Panalytical, Grovewood Rd, WR14 1XZ, Great Malvern, Worcestershire, UK). The samples were dispersed in water and vortexed for 30 seconds before the analysis. Five measurements of 90 seconds each were performed for each sample, and then the data were analyzed using NTA software 3.0.

The morphology of SFNs was investigated by field emission scanning electron microscopy (GeminiSEM-360, Carl Zeiss S.p.A., Milan, Italy). Samples were observed as dried powder previously Pt-sputter-coated (4 nm thick Pt layer) under argon. The samples were imaged at acceleration voltages ranging from 5 to 6 kV, using the InLens SE detector and working distances of 2.0 to 2.9 mm.

ζ-potential was measured using ZetaSizer Nano-ZS90 instrument (Malvern Panalitical, Lissone, MB, Italy). The samples were prepared at 0.5 mg mL^{-1} concentration in PBS buffer 0.01 M, pH 7.4.

Mid-infrared spectra were acquired on a Bruker Alpha II instrument (Bruker, Ettlingen, Germany) equipped with an attenuated total reflection (ATR) accessory featuring a monolithic diamond crystal and a DTGS (deuterated triglycine sulfate) detector, operating in the 4000–450 cm^{-1} range at a resolution of 4 cm^{-1}. OPUS Software (Release 8.7) was used for processing ATR-FTIR spectra.

Release studies were performed using the dialysis technique method.[30] Briefly, 10 mg of nanoparticles (SFNs-BSH and SFNs-N-BSH) from each batch were suspended in 3 mL of PBS and put into a dialysis membrane (3.5 kDa MWCO). The dialysis bags were then immersed in 20 mL of PBS and maintained under gentle magnetic stirring at room temperature. At each selected time point, 2 mL of the release medium was withdrawn and replaced with fresh PBS to maintain sink conditions. The amount of drug released was quantified by ICP-OES, as previously described for the loading determination. Results were expressed as the cumulative release percentage, calculated assuming that 100% release corresponds to the total amount of drug loaded.

The suitability of the formulations for parenteral injection was demonstrated by measuring the residual humidity, osmolarity, and pH of the reconstituted product. The residual humidity was measured by a Coulometric Titrator HI904 (Hanna Instruments, Villafranca Padovana, Italy) after allowing the samples to rebalance at room temperature. The osmolarity was measured using a micro osmometer (Precision System Inc., Natick, MA) after reconstitution of 10 mg of lyophilized SFNs in 2 mL saline (0.9% w/v NaCl in deionized water) at 37 °C. The pH of the reconstituted product was measured by a pH meter (Mettler-Toledo, US).

4.3. Cell treatment and boron concentration measurements

The cytocompatibility of SFNs was assessed on the U87 glioma cell line and human dermal fibroblasts. Both cell types were cultured adherently in T-75 flasks at 37 °C and 5% CO_2. U87 cells were maintained in DMEM supplemented with 10% FBS and 1% gentamicin, while fibroblasts were cultured in DMEM high glucose with the same supplements. Then, an MTT assay was performed as previously reported,[30,41,44] testing SFNs-BSH

and SFNs-N-BSH at 200, 400, 600, and 800 μg mL^{-1}. Cells not treated were used as a control (100% viability).

Uptake studies were performed using the U87 cell line incubated with SFNs-BSH or SFNs-N-BSH at a concentration of 400 μg mL^{-1} for 60 minutes. After incubation, the medium was removed, and the cells were washed three times with PBS, detached by trypsinization, and counted. A total of 4×10^6 cells were collected and centrifuged (1200*g* for 10 minutes) to form a compact pellet, which was placed on a Mylar support and left to dry overnight. The boron concentration was then measured with the nuclear method of neutron autoradiography. Quantitative and qualitative boron uptake analyses were performed at the LENA laboratory (Pavia, Italy), where a well-characterized thermal neutron facility is available at the TRIGA Mark II research reactor.[52] Neutron autoradiography employs a solid-state nuclear track detector (SSNTD), a passive detector that produces an imprinted image of the boron nuclei present in the sample, as previously described.[53] Cell pellets were irradiated in a neutron flux of 2×10^{10} cm^{-2} s^{-1} obtained at the bottom of the TRIGA Mark II thermal column, with the reactor working at 250 kW for 2 hours; the alpha particles and lithium ions generated by the neutron capture in ^{10}B present in the sample damage the SSNTD, which consists of latent tracks that were revealed by a chemical solution (NaOH 0.14 M at 70 °C for 20 minutes). Macroscopic images (30 and 50 mm^2) of the entire sample were obtained using light microscopy; calibration was previously established by quantifying the grey intensity in cell samples with known boron concentrations (standard samples prepared with a known concentration of BPA). Finally, the quantitative distribution was imaged by assessing the grey intensity of each image across the entire pellet area and transformed into a map of ^{10}B concentration. Results were compared to BPA uptake in the same cell line, which was treated with the same procedure, using the optimized parameters (80 ppm of ^{10}B in the culture medium for a 4-hour contact time).

Author contributions

Conceptualization: L. P., ML. T.; formal analysis: I. P.; funding acquisition: L. P., S. B.; investigation: E. B., L. C., C. F., I. M.; methodology: E. B.; I. P., L. C., C. F., project administration: L. P., D. I., resources: L. P., ML. T., supervision: D. I., S. B.; validation: E. B., I. M., D. I., C. F. visualization: D. I., I. M., writing – original draft: E. B., D. I., I. M., S. B., L. C.; writing – review & editing: D. I., I. M., ML. T, S. B., Y-H. L., L. P., Y. Z.

Conflicts of interest

There are no conflicts to declare.

Data availability

The data supporting this article have been included as part of the SI. Supplementary information: Scheme of the process of preparation, characterization and testing of SFNs-BSH and SFNs-N-BSH; EDX spectra of SFNs-BSH and SFNs-N-BSH; Representative FESEM images of bare SFNs; Example of boron quantification in U-87 cells treated with BPA. See DOI: **https://doi.org/10.1039/d5ma00336a**.

Acknowledgements

This work was supported in part by the Italian Ministry of Foreign Affairs and International Cooperation, grant numbers CN24GR05 and CN23GR01 (AMONG-US). Dr Chiara Zaccone is gratefully acknowledged for the support in ICP-OES analysis.

References

1 A. Monti Hughes and N. Hu, *Cancers*, 2023, **15**, 4091.
2 K. Hirose and M. Sato, *Int. J. Radiat. Oncol., Biol., Phys.*, 2024, **120**, 796–804.
3 W. H. Jin, C. Seldon, M. Butkus, W. Sauerwein and H. B. Giap, *Int. J. Part Ther.*, 2022, **9**, 71–82.
4 M. Sato, K. Hirose, S. Takeno, T. Aihara, K. Nihei, Y. Takai, T. Hayashi, K. Bando, H. Kimura, K. Tsurumi and K. Ono, *Cancers*, 2024, **16**, 869.
5 F. Ali, N. S. Hosmane and Y. Zhu, *Molecules*, 2020, **25**, 828.
6 D. Skwierawska, J. A. López-Valverde, M. Balcerzyk and A. Leal, *Cancers*, 2022, **14**, 2865.
7 H. Xu, J. Liu, R. Li, J. Lin, L. Gui, Y. Wang, Z. Jin, W. Xia, Y. Liu, S. Cheng and Z. Yuan, *Coord. Chem. Rev.*, 2024, **511**, 215795.
8 D. Imperio and L. Panza, *Symmetry*, 2022, **14**, 182.
9 B. Muz, A. K. Azab, L. Confalonieri, E. Del Grosso, S. Fallarini, D. Imperio and L. Panza, *Bioorg. Med. Chem.*, 2022, **59**, 116659.
10 J. Matović, K. Bahrami, P. Stockmann, I. K. Sokka, Y. C. Khng, M. Sarparanta, E. Hey-Hawkins, J. Rautio and F. S. Ekholm, *Mol. Pharmacol.*, 2023, **20**, 3127–3139.
11 L. Confalonieri, D. Imperio, A. Erhard, S. Fallarini, F. Compostella, E. del Grosso, M. Balcerzyk and L. Panza, *ACS Omega*, 2022, **7**, 48340–48348.
12 S. Villani, D. Imperio, L. Panza, L. Confalonieri, S. Fallarini, S. Aprile and E. Del Grosso, *Eur. J. Med. Chem.*, 2024, **279**, 116844.
13 J. Järvinen, H. Pulkkinen, J. Rautio and J. M. Timonen, *Pharmaceutics*, 2023, **15**, 2663.
14 D. O. Zharkov, A. V. Yudkina, T. Riesebeck, P. S. Loshchenova, E. A. Mostovich and G. L. Dianov, *Am. J. Cancer Res.*, 2021, **11**, 4668–4682.
15 S. O. Oloo, K. M. Smith, M. da and G. H. Vicente, *Cancers*, 2023, **15**, 3277.
16 M. J. Luderer, B. Muz, K. Alhallak, J. Sun, K. Wasden, N. Guenthner, P. de la Puente, C. Federico and A. K. Azab, *Pharm. Res.*, 2019, **36**, 144.
17 R. Li, J. Zhang, J. Guo, Y. Xu, K. Duan, J. Zheng, H. Wan, Z. Yuan and H. Chen, *Mol. Pharmacol.*, 2020, **17**, 202–211.

18 T. H. Bünning, L. Panza, A. K. Azab, B. Muz, S. Fallarini and D. Imperio, *Symmetry (Basel)*, 2021, **13**, 202.
19 I. Fuentes, T. García-Mendiola, S. Sato, M. Pita, H. Nakamura, E. Lorenzo, F. Teixidor, F. Marques and C. Viñas, *Chem. – Eur. J.*, 2018, **24**, 17239–17254.
20 S. Gimondi, H. Ferreira, R. L. Reis and N. M. Neves, *Int. J. Mol. Sci.*, 2023, **25**, 312.
21 S. Behzadi, V. Serpooshan, W. Tao, M. A. Hamaly, M. Y. Alkawareek, E. C. Dreaden, D. Brown, A. M. Alkilany, O. C. Farokhzad and M. Mahmoudi, *Chem. Soc. Rev.*, 2017, **46**, 4218–4244.
22 M. J. Mitchell, M. M. Billingsley, R. M. Haley, M. E. Wechsler, N. A. Peppas and R. Langer, *Nat. Rev. Drug Discovery*, 2021, **20**, 101–124.
23 M. A. Subhan, S. S. K. Yalamarty, N. Filipczak, F. Parveen and V. P. Torchilin, *J. Pers. Med.*, 2021, **11**, 571.
24 R. Bajracharya, J. G. Song, B. R. Patil, S. H. Lee, H.-M. Noh, D.-H. Kim, G.-L. Kim, S.-H. Seo, J.-W. Park, S. H. Jeong, C. H. Lee and H.-K. Han, *Drug Delivery*, 2022, **29**, 1959–1970.
25 F. Tamanoi, S. Chinnathambi, M. Laird, A. Komatsu, A. Birault, T. Takata, T. L.-H. Doan, N. X. D. Mai, A. Raitano, K. Morrison, M. Suzuki and K. Matsumoto, *Int. J. Mol. Sci.*, 2021, **22**, 2251.
26 J. Li, O. Janoušková, R. Fernandez-Alvarez, S. Mesíková, Z. Tošner, S. Kereïche, M. Uchman and P. Matějíček, *Chem. – Eur. J.*, 2020, **26**, 14283–14289.
27 S. Hirase, A. Aoki, Y. Hattori, K. Morimoto, K. Noguchi, I. Fujii, T. Takatani-Nakase, S. Futaki, M. Kirihata and I. Nakase, *Mol. Pharmacol.*, 2022, **19**, 1135–1145.
28 G. Ailuno, A. Balboni, G. Caviglioli, F. Lai, F. Barbieri, I. Dellacasagrande, T. Florio and S. Baldassari, *Cells*, 2022, **11**, 4029.
29 T. Yamamoto, K. Nakai and A. Matsumura, *Cancer Lett.*, 2008, **262**, 143–152.
30 M. Ueno, H. S. Ban, K. Nakai, R. Inomata, Y. Kaneda, A. Matsumura and H. Nakamura, *Bioorg. Med. Chem.*, 2010, **18**, 3059–3065.
31 M. Laird, K. Matsumoto, Y. Higashi, A. Komatsu, A. Raitano, K. Morrison, M. Suzuki and F. Tamanoi, *Nanoscale Adv.*, 2023, **5**, 2537–2546.
32 X. Zhang, L. M. Rendina and M. Müllner, *ACS Polymers Au*, 2024, **4**, 7–33.
33 B. Crivelli, E. Bari, S. Perteghella, L. Catenacci, M. Sorrenti, M. Mocchi, S. Faragò, G. Tripodo, A. Prina-Mello and M. L. Torre, *Eur. J. Pharm. Biopharm.*, 2019, **137**, 37–45.
34 M. A. Asensio Ruiz, M. G. Fuster, T. Martínez Martínez, M. G. Montalbán, J. L. Cenis, G. Víllora and A. A. Lozano-Pérez, *Polymers*, 2022, **14**, 498.
35 B. O. Ode Boni, B. M. Bakadia, A. R. Osi, Z. Shi, H. Chen, M. Gauthier and G. Yang, *Macromol. Biosci.*, 2022, **22**(1), 2100292.
36 C. N. Pace, F. Vajdos, L. Fee, G. Grimsley and T. Gray, *Protein Sci.*, 1995, **4**, 2411–2423.
37 B. Mao, C. Liu, W. Zheng, X. Li, R. Ge, H. Shen, X. Guo, Q. Lian, X. Shen and C. Li, *Biomaterials*, 2018, **161**, 306–320.
38 F. Mottaghitalab, M. Kiani, M. Farokhi, S. C. Kundu, R. L. Reis, M. Gholami, H. Bardania, R. Dinarvand, P. Geramifar, D. Beiki and F. Atyabi, *ACS Appl. Mater. Interfaces*, 2017, **9**, 31600–31611.
39 B. Liu, P. Wu, H. Sha, H. Qian, Q. Wang, Y. Yang, M. Yang, X. Bian and L. Cheng, *Onco Targets Ther*, 2016, 3153.
40 S. Gou, Y. Huang, Y. Wan, Y. Ma, X. Zhou, X. Tong, J. Huang, Y. Kang, G. Pan, F. Dai and B. Xiao, *Biomaterials*, 2019, **212**, 39–54.
41 A. Rodriguez-Nogales, F. Algieri, L. De Matteis, A. A. Lozano-Perez, J. Garrido-Mesa, T. Vezza, J. M. de da Fuente, J. L. Cenis, J. Galvez and M. E. Rodriguez-Cabezas, *Int. J. Nanomed.*, 2016, **11**, 5945–5958.
42 F. Mottaghitalab, M. Farokhi, M. A. Shokrgozar, F. Atyabi and H. Hosseinkhani, *J. Controlled Release*, 2015, **206**, 161–176.
43 E. Bari, M. Serra, M. Paolillo, E. Bernardi, S. Tengattini, F. Piccinini, C. Lanni, M. Sorlini, G. Bisbano, E. Calleri, M. L. Torre and S. Perteghella, *Cancers*, 2021, **13**, 1185.
44 V. Pirota, G. Bisbano, M. Serra, M. L. Torre, F. Doria, E. Bari and M. Paolillo, *Cancers*, 1725, **2023**, 15.
45 F. Ferrera, R. Resaz, E. Bari, D. Fenoglio, L. Mastracci, I. Miletto, A. Modena, S. Perteghella, M. Sorlini, L. Segale, G. Filaci, M. L. Torre and L. Giovannelli, *Int. J. Biol. Macromol.*, 2024, **282**, 137121.
46 M. A. Gadan, R. Lloyd, G. Saint Martin, M. S. Olivera, L. Policastro and A. M. Portu, *Microsc. Microanal.*, 2019, **25**, 1331–1340.
47 K. Yokoyama, S.-I. Miyatake, Y. Kajimoto, S. Kawabata, A. Doi, T. Yoshida, T. Asano, M. Kirihata, K. Ono and T. Kuroiwa, *J. Neurooncol.*, 2006, **78**, 227–232.
48 E. Bari, F. Ferrera, T. Altosole, S. Perteghella, P. Mauri, R. Rossi, G. Passignani, L. Mastracci, M. Galati, G. I. Astone, M. Mastrogiacomo, P. Castagnola, D. Fenoglio, D. Di Silvestre, M. L. Torre and G. Filaci, *J. Immunother. Cancer*, 2023, **11**, e005916.
49 K. Jiang, A. Loni, L. T. Canham and J. L. Coffer, *Phys. Status Solidi A*, 2009, **206**, 1361–1364.
50 G. Socrates, *Infrared and Raman Characteristic Group Frequencies Tables and Charts*, John Wiley &sons LTD, Chichester, England, 2001, pp. 247–253.
51 A. D. Ready, S. M. Becwar, D. Jung, A. Kallistova, E. Schueller, K. P. Anderson, R. Kubena, R. Seshadri, B. F. Chmelka and A. M. Spokoyny, *Dalton Trans.*, 2022, **51**, 11547–11557.
52 S. Bortolussi, N. Protti, M. Ferrari, I. Postuma, S. Fatemi, M. Prata, F. Ballarini, M. P. Carante, R. Farias, S. J. González, M. Marrale, S. Gallo, A. Bartolotta, G. Iacoviello, D. Nigg and S. Altieri, *Nucl. Instrum. Methods Phys. Res. B*, 2018, **414**, 113–120.
53 I. Postuma, S. Bortolussi, N. Protti, F. Ballarini, P. Bruschi, L. Ciani, S. Ristori, L. Panza, C. Ferrari, L. Cansolino and S. Altieri, *Rep. Pract. Oncol. Radiother.*, 2016, **21**, 123–128.